Acta Pharmacologica Sinica

www.nature.com/aps

ARTICLE

Berberine remodels adipose tissue to attenuate metabolic disorders by activating sirtuin 3

Dan Li[1,2], Chao Yang[2,3], Jian-zhong Zhu[2], Eduardo Lopez[4], Tian Zhang[2], Qiang Tong[4], Cheng Peng[1] and Li-gen Lin[2]

Adipose tissue remodelling is considered a critical pathophysiological hallmark of obesity and related metabolic diseases. Berberine (BBR), a natural isoquinoline alkaloid, has potent anti-hyperlipidaemic and anti-hyperglycaemic effects. This study aimed to explore the role of BBR in modulating adipose tissue remodelling and the underlying mechanisms. BBR protected high fat diet (HFD)-fed mice against adiposity, insulin resistance and hyperlipidemia. BBR alleviated adipose tissue inflammation and fibrosis by inhibiting macrophage infiltration, pro-inflammatory macrophage polarization and the abnormal deposition of extracellular matrix, and the effect was mediated by BBR directly binding and activating the deacetylase Sirtuin 3 (SIRT3) and suppressing the activation of the mitogen-activated protein kinases and nuclear factor-κB signalling pathways. Furthermore, BBR decreased microRNA-155-5p secretion by macrophages, which in turn ameliorated liver injury. Moreover, BBR mitigated inflammatory responses in both LPS-stimulated macrophages and TNF-α-treated adipocytes and suppressed macrophage migration towards adipocytes by activating SIRT3. Collectively, this study revealed that BBR improved adipose tissue remodelling, and subsequently inhibited the secretion of microRNA-155-5p by macrophages, which alleviated adiposity, insulin resistance and liver injury in obese mice. The modulation of adipose tissue remodelling by activating SIRT3 could contribute to the anti-hyperlipidemic and anti-hyperglycemic effects of BBR.

Keywords: berberine; adipose tissue inflammation; fibrosis; liver injury; Sirtuin 3; insulin resistance.

Acta Pharmacologica Sinica (2022) 43:1285–1298; https://doi.org/10.1038/s41401-021-00736-y

INTRODUCTION

According to 2020 World Health Organization report, overweight or obesity causes more than 2.8 million people to die each year. Obesity is usually characterized by excessive lipid accumulation in adipose tissue and ectopic fat deposition in other organs and is positively correlated with cardiovascular diseases, type 2 diabetes, and non-alcoholic fatty liver disease (NAFLD) [1]. Under excess nutrient conditions, adipose tissue rapidly and dynamically remodels through adipocyte hypertrophy and hyperplasia [2], accompanied by elevated immune cell accumulation, the overproduction of extracellular matrix (ECM), and subsequent pro-inflammatory responses in obese fat pads [3]. Subsequently, adipose tissue inflammation and fibrosis cause liver injury and systemic insulin resistance (IR) [4].

Adipose tissue macrophages (ATMs) are the predominant leukocytes in adipose tissue, which make up approximately 5% of lean adipose tissue, and these cells notably increase up to 50% in the adipose tissue of obese rodents and humans [5]. In addition to the increased number of ATMs, the alternatively activated macrophage (M2) phenotype shifts to the classically activated macrophage (M1) phenotype in the obese state [6]. M1 ATMs secrete a variety of cytokines including IL-6 and TNF-α, and chemokines, such as macrophage inflammatory protein-1α (MIP-1α) and monocyte chemoattractant protein-1 (MCP-1), which result in low-grade chronic inflammation [7]. Hypertrophic adipocytes are more common in obese subjects [4], and ECM components including collagen and fibronectin provide mechanical support for the physiological expansion of adipose tissue. However, the abnormal obesity-induced production and deposition of ECM leads to decreased tissue flexibility and the destruction of normal adipose tissue structure [8]. Hypertrophic adipocytes without proper ECM support result in adipocyte stress and death and the formation of inflammatory foci, which in turn attract more macrophage accumulation in adipose tissue and exacerbate the local inflammatory response [9]. Thus, ameliorating adipose tissue inflammation and abnormal ECM deposition may provide a promising therapeutic strategy for the treatment of metabolic diseases.

Berberine (BBR), a well-known natural bioactive isoquinoline alkaloid in quaternary ammonium salt forms [10], exhibits excellent performance on the treatment of IR, obesity, diabetes, hyperlipidemia, and fatty liver disease [11]. Herein, high-fat diet (HFD)-induced obese mice were used to investigate the effects and underlying mechanisms of BBR in modulating adipose tissue remodelling and protecting the liver against lipotoxicity.

[1]State Key Laboratory of Southwestern Chinese Medicine Resources, School of Pharmacy, Chengdu University of Traditional Chinese Medicine, Chengdu 610075, China; [2]State Key Laboratory of Quality Research in Chinese Medicine, Institute of Chinese Medical Sciences, University of Macau, Taipa, Macau, China; [3]Key Laboratory of Health Risk Factors for Seafood and Environment of Zhejiang Province, Institute of Innovation & Application, Zhejiang Ocean University, Zhoushan 316022, China and [4]Children's Nutrition Research Center, Department of Pediatrics, Baylor College of Medicine, Houston, TX, USA
Correspondence: Cheng Peng (pengchengchengdu@126.com) or Li-gen Lin (ligenl@um.edu.mo)
These authors contributed equally: Dan Li, Chao Yang

Received: 6 March 2021 Accepted: 29 June 2021
Published online: 20 August 2021

MATERIALS AND METHODS

Ethic

All in vivo experiments and primary cultures were conducted under the regulation of the Animal Ethics and Welfare Committee of University of Macau (No. ICMS-AEC-2014-06) and conformed to the ARRIVE guidelines. Mice were obtained from the Faculty of Health Science, University of Macau (Macau, China) and were maintained on a 12 h light/12 h dark cycle with air filtration under controlled temperature (22 ± 2 °C) in plastic cages. Food and water were available *ad libitum*.

Animal experimental procedure

To establish the model of diet-induced obesity, male C57BL/6 J mice aged 8 to 10 weeks were randomly assigned to a regular chow diet (RD group, calorie 2.35 kcal/g) or a 45% high fat diet (HFD, calorie 4.5 kcal/g, Trophic Animal Feed High-Tech Co., Nantong, Jiangsu, China). The RD group and one group of HFD-fed mice were administered with sterile distilled deionized water (10 mL/kg body weight) via oral gavage, and the other group of HFD-fed mice were treated intragastrically with a BBR solution (200 mg/kg body weight, dissolved in sterile distilled deionized water) once per day for 20 weeks. The mice were euthanized, and blood samples were collected. After the mice were sacrificed, epididymal white adipose tissues (eWAT) and the liver were dissected and divided into several fragments. One part of the eWAT was used to isolate the stromal vascular fraction (SVF), another part of the eWAT and liver were fixed in 4% paraformaldehyde, and the rest of the tissues was quickly frozen in liquid nitrogen and preserved at −80 °C for subsequent analyses.

Cell culture

RAW264.7 macrophages (American Type Culture Collection, ATCC, Manassas, VA, USA) were cultured in DMEM with 10% foetal bovine serum (FBS, Thermo-Fisher, Waltham, MA, USA), and 3T3-L1 preadipocytes (ATCC) were cultured in DMEM with 10% calf serum (CS, Thermo-Fisher) as previously reported [12]. Macrophages at passages 5–15 and preadipocytes at passages 7–10 were used in the experiments. For adipocyte differentiation, 3T3-L1 cells were stimulated for 72 h with dexamethasone (1 μM, Sigma-Aldrich, St Louis, MO, USA), 1-methyl-3-isobutylxanthine (IBMX, 0.5 mM, Sigma-Aldrich), and insulin (5 μg/mL, Sigma-Aldrich) in DMEM supplemented with 10% FBS and were subsequently incubated with 5 μg/mL insulin for 5 days. The growth medium was exchanged every other day during the course of differentiation. On the 8th day of differentiation, the adipocytes were pretreated with BBR for 6 h and then challenged with TNF-α (15 ng/mL, Sigma-Aldrich) for the indicated time.

Differentiation of bone marrow-derived macrophages (BMDMs)

BMDMs were isolated from the bone marrow of male C57BL/6 J mice (6–8 weeks old) and cultured in RPMI-1640 supplemented with 10% FBS and 20% L929 cell (Stem Cell Bank, Chinese Academy of Sciences)-conditioned medium for 7 days [13]. Subsequently, the differentiated BMDMs were treated with BBR (80 μM) for 1 h and then stimulated with lipopolysaccharide (LPS, 1 μg/mL, Sigma-Aldrich) for the indicated time.

Knockdown of SIRT3 in macrophages

The reagents (sc-61556-SH, sc-108060 and sc-108061) used in knockdown experiments were purchased from Santa Cruz Biotechnology (Santa Cruz, CA, USA). A total of 4 μg of shRNA was transfected into RAW264.7 macrophages (50% confluent) for 6 h according to the manufacturer's instructions, after which the cells were incubated with fresh cell culture medium for an additional 42 h. Then, the cells were selected using puromycin (10 μg/mL, Thermo-Fisher) for 2 weeks, and the efficiency of SIRT3 knockdown was assessed by Western blotting. Afterwards, macrophages with SIRT3 silencing were used for further experiments.

Cell viability assay

Cells were placed into 96-well plates and cultured overnight. Following treatment with different concentrations of BBR (0–160 μM) or AGK7 (0–20 μM) with or without LPS (1 μg/mL) or TNF-α (15 ng/mL) for 24 h, 10 μL of MTT (5 mg/mL in PBS) was added to each well and incubated for 4 h. Then, the dark blue formazan products were solubilized with DMSO, and the absorbance was determined at 570 nm by using SpectraMax M5 microplate reader (Molecular Devices, USA).

Isolation of the SVF and flow cytometry

The SVF was isolated from eWAT using the following steps [13]. The dissected eWAT was digested for 40 min with shaking at 37 °C in Krebs-Ringer bicarbonate (KRB) buffer with 1 mg/mL type I collagenase (Worthington Biochemical Corporation, NJ, USA). The digested cell mixture was collected by using a 100 μm cell strainer (BD Bioscience, San Jose, CA, USA). SVF pellets were harvested after centrifugation at 1200 r/min for 5 min at 4 °C and then resuspended in PBS. The cells were lysed with 1× Red Blood Cell Lysis Buffer (BD Bioscience), resuspended in PBS, and analysed with Accur C6 flow cytometer (BD Bioscience).

Metabolic assays

Insulin tolerance tests (ITTs) and glucose tolerance tests (GTTs) were conducted as previously reported [14]. For the GTTs, the mice were fasted for 16 h, and a glucose (Sigma-Aldrich) solution (2.0 g/kg body weight) was intraperitoneally injected. For the ITTs, the mice were fasted for 6 h, and human insulin (0.75 U/kg body weight) was administered by an intraperitoneal injection. Tail blood glucose was measured at 0, 15, 30, 60, 90, and 120 min by using a OneTouch Ultra blood glucose meter and LifeScan test strips.

Commercial kits (Nanjing Jiancheng Bioengineering Institute, Nanjing, Jiangsu, China) were used to measure the levels of total cholesterol (TC), triglycerides (TGs), high-density lipoprotein-cholesterol (HDL-C), low-density lipoprotein-cholesterol (LDL-C), non-esterified fatty acids (NEFAs), aspartate aminotransferase (AST) and alanine aminotransferase (ALT) in the liver or serum.

Histochemical analysis

Whole-mount histochemical analysis of eWAT and liver tissue was carried out as previously described [13]. Adipocyte areas were measured as described previously [8]. Specific histological features of liver injury were evaluated and scored (grade 0–4) according to the severity of portal inflammation and fibrosis as previously reported [13].

Immunohistochemical analysis

Immunohistochemical analysis of eWAT sections was performed as described previously [15]. After recover antigenicity, the tissue sections were immersed in a 3% H_2O_2 solution for 15 min to quench peroxidase and blocked with 10% BSA (Sigma-Aldrich) in PBS to minimize nonspecific binding. The fat tissue sections were incubated with antibodies against CD11c (1:400 dilution), MMP-9 (1:400 dilution), tissue inhibitor of metalloproteinase 1 (TIMP-1, 1:200 dilution), and α-smooth muscle actin (α-SMA, 1:200 dilution) in PBS containing 3% BSA and 0.1% Tween-20 (Sigma-Aldrich) for 16 h at 4 °C. The sections were washed and subsequently incubated with anti-rabbit or anti-mouse IgG secondary antibodies (Cell Signalling Technology) for 30 min at room temperature. Positive immunoreactivity was visualized by the dark brown colour of the DAB reaction product (Nanjing Jiancheng Bioengineering Institute). The tissue sections were briefly counterstained in haematoxylin, cleared with xylene, and mounted under a cover slip. All positive staining was recognized by comparison with the negative controls, which were stained with nonimmune rabbit or mouse isotype control IgG (vector) under the same conditions. Immunohistochemical images were acquired and analysed by

using a Nikon digital camera attached to a Nikon microscope (Nikon, Tokyo, Japan).

Immunohistofluorescence analyses

Immunohistofluorescence analysis of tissue sections was performed as described previously [12]. After deparaffinization and rehydration, tissue sections were incubated with 10 mM citric acid (pH 6.0), heated in a water bath to recover antigenicity, and blocked with 10% BSA in PBS for 1 h at room temperature to minimize nonspecific binding. eWAT sections and liver tissue sections were stained with primary antibodies against perilipin 1 (1:100, CST), F4/80 (1:400), perilipin 2 (1:100, Proteintech Group) and collagen I (1:400, Abcam). For immunohistofluorescence analysis, macrophages were treated with BBR (80 μM) or BBR (80 μM) + AGK7 (5 μM) for 1 h and subsequently induced with LPS (1 μg/mL) for 1 h. The cells were immediately fixed in 4% formaldehyde. Subsequent procedures were performed as described previously [12]. The stained slides were analysed by a confocal fluorescence microscope (Leica, Germany).

Chemotaxis migration assay

Mature 3T3-L1 adipocytes in DMEM (serum free, 0.2% BSA) were used to prepare conditioned media (CM). RAW264.7 macrophages were pretreated with or without BBR (80 μM) in DMEM with 0.2% BSA for 4 h, and then 5×10^4 cells were placed in the upper wells. Adipocyte CM (0.5 mL) was placed in the lower chamber. The plates were incubated for 4 h at 37 °C, and the macrophages were then fixed, washed, stained with DAPI and observed under a microscope.

RAW264.7 macrophages were seeded into the upper chamber at a density of 5×10^4 cells per well. Fully differentiated adipocytes were treated with BBR (80 μM) for 6 h and then incubated with TNF-α for 24 h. Afterwards, the CM was transferred to the bottom wells of the chemotaxis plates and incubated. The macrophages in the lower compartment were examined.

Determination of nitric oxide (NO) and cytokine levels

The cell culture supernatant was collected to detect NO production by Griess reagents (Sigma-Aldrich) and cytokines (TNF-α, IL-6 and MCP-1) by ELISA kits (Neobiosciences, Shenzhen, China).

qRT-PCR

qRT-PCR analysis was performed as described previously [12, 16]. The relative level of miRNAs was normalized to *U6* snRNA (Thermo-Fisher) and calculated using the $2^{-\Delta\Delta Ct}$ method. The primer information was shown in Supplementary Information Tables S1 and S2.

Western blot analysis

Western blot analysis was carried out as described previously [12]. The immunoblots were analysed using SuperSignal West Femto Maximum Sensitivity Substrate (Thermo-Fisher) and a ChemiDoc™ MP Imaging System (Bio-Rad). The antibody information was shown in Supplementary Information Table S3.

Mitochondrial isolation

Mitochondria were isolated from RAW264.7 macrophages or differentiated 3T3-L1 adipocytes by using the Cell Mitochondria Isolation Kit (Beyotime, Shanghai, China) according to the manufacturer's instructions. The pellet was resuspended in fresh mitochondrial lysis buffer. The mitochondrial isolate was used for Western blot analysis.

SIRT3 deacetylation activity

The SIRT3 deacetylation activity in cell lysates was examined by using a SIRT3 Fluorometric Assay Kit (Sigma-Aldrich). The fluorescence intensity at 460 nm under 360 nm excitation was recorded with a SpectraMax M5 microplate reader (Molecular Devices, USA). All values from each sample are represented as percentages of the control group.

Cellular thermal shift assay (CETSA)

The CESTA was performed as previously reported [17, 18]. Macrophages were preincubated with or without 80 μM BBR for 12 h, and then the cell lysates were collected and analysed with a BCA Protein Assay Kit (Thermo-Fisher), and the concentration was adjusted to 2 μg/μL. The respective lysates were divided into smaller aliquots (50 μL) and heated individually for 5 min using a thermal cycler (Eppendorf, Hamburg, Germany) at different temperatures (50–90 °C). The samples were collected by high-speed centrifugation at 15,000 r/min at 4 °C for 30 min for Western blot analysis.

Molecular docking and dynamics

The possible binding conformation of BBR to SIRT3 was simulated by molecular docking. Despite its lower resolution, the crystal structure of hSIRT3 (PDB ID: 5H4D) in complex with the specific agonist amiodarone was chosen due to the presence of both substrate and NAD^+, and amiodarone was used to define the binding site. Molecular dynamics was performed in GROMACS using the Amber14sb force field [19]. The AM1-BCC [20] partial charge was assigned using the *antechamber* program of AmberTools18. Parameters for the ligand were taken from the general amber force field [21]. Amber topology/coordinate files were acquired by *parmchk2*, *tleap* and were further converted to the GROMACS format using the *acpype* python script. The system was solvated in TIP3P [22] water, neutralized by adding Na^+ or Cl^-, and pre-equilibrated at 310 K and 1 bar by NVT and NPT ensembles. Production was run for 50 ns. The interaction energy between the substrate and SIRT3 was determined by rerunning the production trajectory and then using the *gmx energy* command.

MitoTracker staining

The MitoTracker Green assay (Beyotime) was used to visualize mitochondria in macrophages and adipocytes. Briefly, cells were incubated with MitoTracker Green (100 nM) for 45 min at 37 °C, then washed with HBSS twice, and the nuclei were stained with Hoechst 33342 (Beyotime). Microscope slides were imaged with a confocal microscope system (Olympus, Tokyo, Japan), and analysed with ImageJ software.

Detection of mitochondrial membrane potential

Mitochondrial membrane potential was examined by the JC-1 assay (Beyotime). The cells were incubated with JC-1 for 30 min at 37 °C in the dark. After being washed three times with PBS, the nuclei were stained with Hoechst 33342 (Beyotime). The slides were observed by a confocal microscope (Olympus, Tokyo, Japan) and analysed with ImageJ software.

Statistical analysis

GraphPad Prism 8.0 software was used for all experimental data analyses, and the data are presented as the mean ± SD. Student's *t*-test for comparisons between two groups and one-way analysis of variance (ANOVA) for multiple comparisons were conducted to evaluate the significant differences. *P* values less than 0.05 were considered statistically significant.

RESULTS

BBR alleviates adiposity, IR and hyperlipidaemia in HFD-challenged mice

An HFD-challenged obese mouse model was used to determine the effects of BBR on the regulation of adipose tissue remodelling, and the experimental procedure is shown in Fig. S1a. BBR significantly reduced body weight since 10 weeks post-

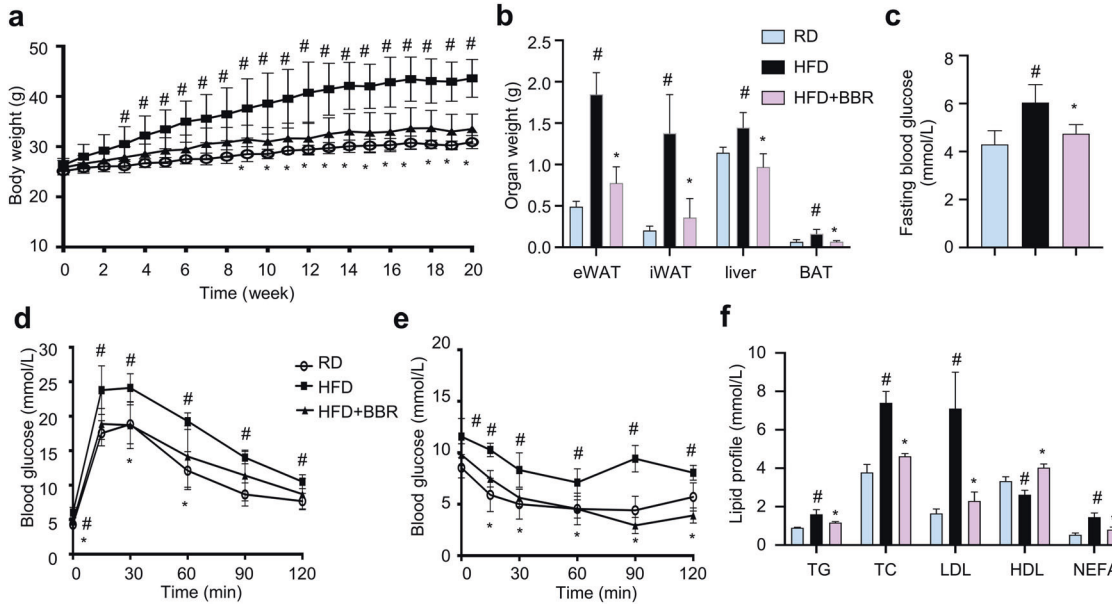

Fig. 1 BBR alleviates adiposity, IR and hyperlipidaemia in HFD-challenged mice. a Body weight in the three groups of mice. **b** Organ weight in the three groups of mice, including that of eWAT, iWAT, the liver and BAT. **c** The blood glucose levels of mice after 16 h of fasting. **d** GTTs were performed 16 weeks post-BBR administration, following 16 h of fasting. **e** ITTs were performed 18 weeks post-BBR administration, following 6 h of fasting. **f** The lipid parameters in serum were measured. The data represent the means ± SD ($n = 8$). $^{\#}P < 0.05$ HFD *vs*. RD, $^{*}P < 0.05$ BBR *vs*. HFD.

administration (Fig. 1a) but did not obviously affect food intake (Fig. S1b) compared to those of HFD-fed mice. BBR treatment obviously reversed HFD-induced increases in the weights and ratios of eWAT, inguinal WAT (iWAT) and brown adipose tissue (BAT), as well as the liver weight (Fig. 1b and S1c). GTTs and ITTs were carried out to estimate the effects of BBR on systemic insulin sensitivity. BBR treatment significantly reduced the fasting blood glucose levels in obese mice (Fig. 1c). In the GTTs, the glucose clearance rate was enhanced by treatment with BBR compared to that of HFD-fed mice (Fig. 1d). Next, the ITTs indicated that BBR treatment increased insulin sensitivity in obese mice (Fig. 1e). Integrated blood glucose levels were estimated by calculating the value of the area under the curve (AUC) and were observably reduced in BBR-treated mice (Fig. S1d, e). In addition, the levels of serum lipid parameters, including TC, TG, LDL-C and NEFA, were markedly reduced in BBR-treated mice (Fig. 1f), and the level of serum HDL-C was obviously increased by BBR (Fig. 1f) compared to those of HFD-fed mice. Taken together, these results suggest that BBR ameliorates adiposity, IR and hyperlipidaemia in HFD-fed mice.

BBR reduces macrophage infiltration into eWAT

H&E staining of eWAT revealed smaller adipocytes in BBR-treated mice than the hypertrophic adipocytes observed in HFD-fed mice (Fig. 2a–c and S2). The mRNA expression levels of iNOS, COX2, TNF-α, IL-1β and IFN-γ were increased in the eWAT of HFD-fed mice and were decreased by the administration of BBR (Fig. 2d), indicating that BBR ameliorated HFD-induced adipose tissue inflammation in mice. Immunohistofluorescent staining of eWAT from obese mice showed more crown-like structures (CLSs) and F4/80-positive macrophages than those from RD mice, while BBR treatment reduced the formation of CLSs and the number of F4/80^{+} macrophages in eWAT (Fig. 2e). Consistently, the mRNA expression levels of macrophage markers, including F4/80 and CD68, and chemokines, including MCP-1, MIP-1α, Ccl5, Ccl11, Cx3cl1 and Cxcl10, were markedly increased in eWAT from HFD-fed mice, and BBR obviously suppressed the expression levels of these genes (Fig. 2f, g), indicating that BBR inhibited macrophage chemotaxis. To test this hypothesis, the effect of CM from differentiated adipocytes on macrophage chemotaxis was evaluated using a Transwell system. The number of migrated cells was significantly reduced by pretreatment with BBR (Fig. S3a). Furthermore, CM from TNF-α-treated adipocytes exacerbated macrophage chemotaxis, and this effect was suppressed by treating TNF-α induced adipocytes with BBR (Fig. S3b), demonstrating that BBR could suppress the TNF-α-induced production of chemoattractants in adipocytes. As expected, BBR decreased the expression of chemokines, including MCP-1, MIP-1α, Ccl5, Cxcl10 and Cx3cl1, in LPS-induced BMDMs (Fig. S3c). Collectively, BBR mitigates adipose tissue inflammation by suppressing macrophage infiltration into eWAT in HFD-fed mice.

BBR prevents M1/M2 macrophage polarization in eWAT

Interestingly, BBR treatment distinctly reduced the mRNA expression of the M1 macrophage marker CD11c (Fig. 2g), and elevated the mRNA expression of the M2 macrophage markers CD206 and CD301 in eWAT (Fig. 2g), which suggested that BBR promoted a shift toward anti-inflammatory M2 polarization. Notably, flow cytometry showed that M1 macrophages (CD11c^{+}CD206^{-}) and double-positive macrophages (CD11c^{+}CD206^{+}) were significantly increased, M2 macrophages (CD11c^{-}CD206^{+}) were reduced in eWAT from HFD-fed mice compared to RD mice, and BBR treatment reversed these changes (Fig. 2h). Consistently, more positive staining of CD11c was visualized in the stromal space of eWAT from HFD mice, and this effect was reversed in BBR-treated mice (Fig. 2i). Exposure to LPS increased the mRNA expression of iNOS, COX2, IL-1, IL-6 and TNF-α (M1 macrophage markers) in BMDMs, and this expression was diminished when BMDMs were pretreated with BBR (Fig. S4a). In contrast, exposure to IL-4 elevated the mRNA expression of CD206, YM-1 and Arg-1 (M2 macrophage markers) in BMDMs, and BBR treatment further augmented this expression (Fig. S4b). Taken together, these data suggest that BBR modulates the ratio of M1 to M2 macrophages in the eWAT of HFD-fed mice.

BBR mitigates the abnormal deposition of ECM components in eWAT

As shown in Fig. 3a, Masson's trichrome staining and Sirius Red staining showed that collagen deposition and the distinct pattern

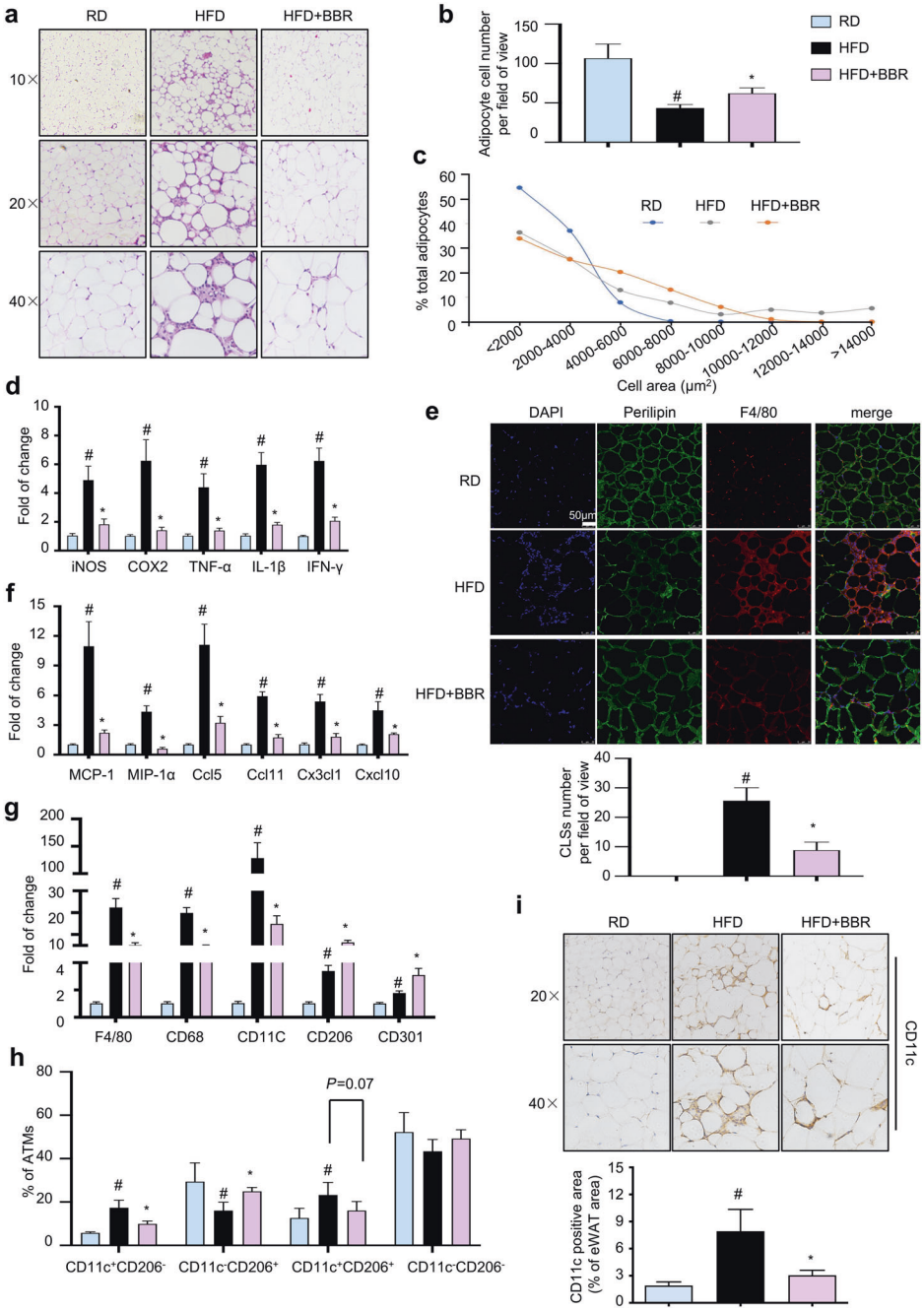

Fig. 2 BBR inhibits macrophage infiltration and pro-inflammatory macrophage polarization in the eWAT of obese mice. a Representative H&E staining images of eWAT. **b** The number of adipocytes per field under 20× view in H&E-stained WAT. **c** Adipocyte size frequency distribution profiles in eWAT. **d** The mRNA expression levels of iNOS, COX2, TNF-α, IL-1β, and IFN-γ in eWAT. **e** F4/80-positive staining in eWAT, scale bar = 50 μm. The number of CLSs per field of view was calculated using ImageJ software. **f** The mRNA expression of MCP-1, MIP-1α, Ccl5, Ccl11, Cx3cl1, and Cxcl10 in eWAT. **g** The mRNA expression of F4/80, CD68, CD11c, CD206, and CD301 in eWAT. **h** The levels of ATM subtypes are represented as ratios to the total population of ATMs. **i** Representative immunohistochemical staining for CD11c. Positive immunostaining is shown in brown. The bar graphs represent the percentage of CD11c-positive stained areas. The data represent the means ± SD ($n = 8$). $^{\#}P < 0.05$ HFD *vs.* RD, $^{*}P < 0.05$ BBR *vs.* HFD.

of collagen distribution in interstitial tissue were increased in the eWAT of HFD-fed mice, and collagen fibres primarily formed in fibrotic bundles surrounding adipocytes in HFD-fed mice. Notably, the abnormal deposition of collagen was attenuated in BBR-treated mice (Fig. 3a). Furthermore, immunofluorescent staining indicated increased collagen I deposition in the eWAT of HFD-fed mice, and BBR greatly reduced collagen I levels (Fig. 3b). Fibrogenic regulators were hardly detected in the fat depots of RD mice (Fig. 3c–f). The intense staining of α-SMA in the eWAT of obese mice indicated increased migration of activated myofibroblast-like cells into adipose tissue, leading to the secretion of more ECM components (Fig. 3c, f), and the intense staining of MMP-9 and TIMP-1 in the regions of macrophage-rich areas indicated that macrophages were involved in ECM component deposition (Fig. 3d, f). The protective effect of BBR on interstitial fibrosis was evidenced by inhibition of the

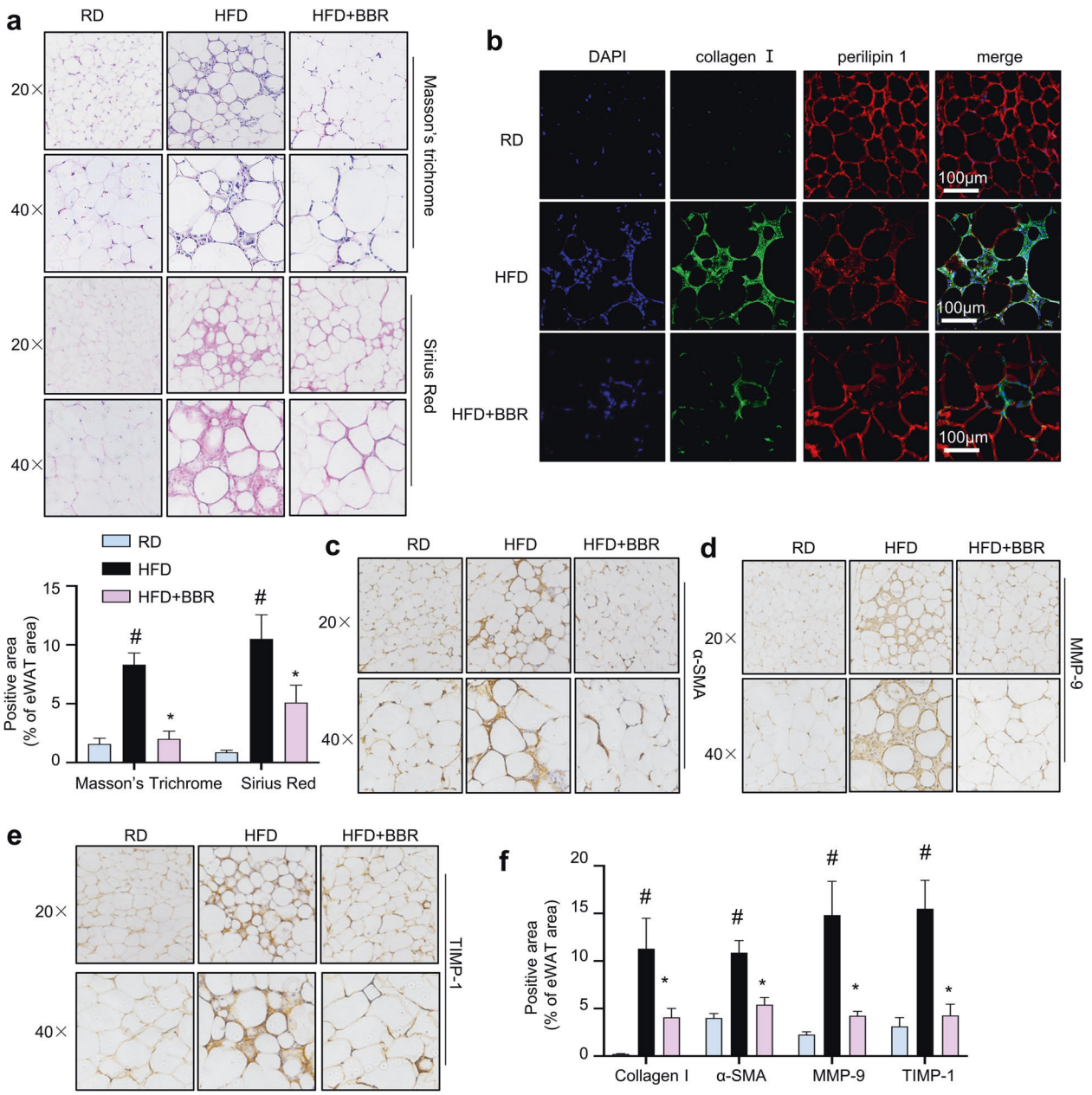

Fig. 3 BBR ameliorates abnormal ECM components in the eWAT of HFD-challenged mice. a Representative images of pathological eWAT abnormalities in mice, as shown by Masson's trichrome staining and Sirius Red staining. Original magnification, ×20 and ×40. The proportion of positive-stained areas to total areas in Masson's trichrome- and Sirius Red-stained eWAT sections were estimated by ImageJ software. **b** Immunofluorescent staining for collagen I (green) and perilipin 1 (red) and nuclear staining with DAPI (blue). Scale bar (white) = 100 μm. **c–e** Immunohistochemical staining of α-SMA, MMP-9 and TIMP-1 in eWAT. **f** The ratios of the positive-stained areas of collagen I, α-SMA, MMP-9 and TIMP-1 to the total tissue area were estimated. The data represent the mean ± SD ($n = 8$). $^{\#}P < 0.05$ HFD *vs*. RD, $^{*}P < 0.05$ BBR *vs*. HFD.

expression levels of ECM components including collagen I, α-SMA, MMP-9, and TIMP-1 (Fig. 3b–f). Collectively, these results suggest that BBR ameliorates abnormal ECM synthesis and deposition in eWAT and consequently induces favourable ECM flexibility, which is beneficial for the healthy expansion of adipose tissue.

BBR attenuates liver injury in HFD-fed mice by suppressing microRNA155-5p expression and secretion by ATMs

Liver injury was evaluated to better understand the beneficial effect of BBR on metabolic disorders. As shown in Fig. 4a, H&E and Masson's trichrome staining indicated that HFD feeding caused worsened hepatic fatty infiltration and collagen production, which were dramatically improved by BBR treatment. Consistently, immunofluorescent staining for collagen I and perilipin 2 showed severe fibrosis and increased lipid accumulation in the livers of obese mice, and BBR treatment significantly reversed hepatic fibrosis and lipid accumulation (Fig. 4b and S5). Furthermore, BBR alleviated the levels of TC, TG, LDL-C and NEFA and elevated the level of HDL-C in the livers of obese mice (Fig. 4c). Additionally, BBR treatment obviously decreased the levels of ALT and AST in the livers of obese mice (Fig. 4d).

microRNA-155-5p (*miR-155-5p*) is induced in macrophages during inflammation [23] and plays a critical role in the pathogenesis of liver steatosis and fibrosis [24]. HFD feeding significantly induced increased *miR-155-5p* expression in the serum and eWAT compared to that of RD mice, and this effect

was completely abrogated in BBR-treated mice (Fig. 4e, f). Consistently, *miR-155-5p* expression in LPS-stimulated BMDMs was significantly decreased by treatment with BBR (Fig. 4g). Thus, BBR attenuates liver injury in HFD-fed mice, which might occur by decreasing *miR-155-5p* secretion from macrophages.

BBR exacerbates SIRT3 activity and inhibits MAPK/NF-κB signalling in eWAT

To elucidate the potential target of BBR, the expression of some key regulators was evaluated. As shown in Fig. 5a, HFD feeding was accompanied by reduced SIRT3 expression in eWAT, and BBR treatment attenuated this change. In RAW264.7 macrophages, BBR markedly increased the SIRT3 protein level but not the expression of Nampt, an enzyme involved in NAD^+ synthesis (Fig. 5b). As expected, BBR reversed the LPS-induced suppression of SIRT3 deacetylation activity, and this effect was abrogated by cotreatment with the selective SIRT3 inhibitor AGK7 (Fig. 5c). The deacetylation activity was further evaluated by examining the acetylation status of MnSOD, a SIRT3 substrate. BBR dose-dependently reduced the acetylation level of MnSOD at K122 (Fig. 5b). Next, mitochondria were isolated from macrophages, and BBR substantially reduced the mitochondrial protein acetylation level (Fig. 5d), which was partially abrogated by cotreatment with cycloheximide, an inhibitor of SIRT3 protein synthesis (Fig. 5e). Next, CETSA was performed on macrophages to further verify that BBR interacts with SIRT3 deacetylase. Likewise, BBR treatment led to enhanced stabilization of SIRT3 compared to that of control cells at a wide variety of temperatures (Fig. 5f). Virtual docking analysis was performed to examine the direct interaction between SIRT3 and BBR. In the crystal structure of SIRT3 (PDB ID: 5H4D), both the acetyl end of the substrate and NAD^+ stretched into the pocket, and BBR was successfully docked at the entrance of the pocket via hydrophobic interactions and hydrogen bonds with residues on both the upper and lower sides (V324, R158, Q228, H248, E323), as well as NAD^+ (Fig. 5g). With the acquired docking conformation, the binding was confirmed by molecular dynamics. The interaction energy between the substrate and SIRT3 was calculated to be −364.379 and −340.331 kJ/mol with or without BBR, respectively (Fig. 5h), indicating that BBR increased the affinity of the substrate for SIRT3. Thus, BBR might directly bind to SIRT3 and enhance its deacetylation activity.

Moreover, HFD feeding observably increased the levels of iNOS and COX-2, and BBR treatment reversed these changes (Fig. 5a). Compared to that of HFD-fed mice, the phosphorylation of ERK, JNK and p38 was significantly suppressed (Fig. 5i), and the phosphorylation of IKKα/β, IκBα and p65 was significantly decreased in the eWAT of BBR-treated mice (Fig. 5j). Thus, BBR inhibits the MAPK/NF-κB signalling pathways in eWAT.

SIRT3 knockdown reverses the inhibitory effect of BBR on inflammatory responses in macrophages

SIRT3 was involved in mediating MAPK and NF-κB signalling activation in inflammatory states [25, 26]. Compared to the vehicle control, LPS treatment suppressed SIRT3 expression and elevated iNOS and COX2 expression, while BBR significantly increased SIRT3 expression and decreased iNOS and COX2 expression in LPS-induced BMDMs (Fig. S6a). LPS induced NF-κB signalling activation in BMDMs, and BBR strongly inhibited the LPS-induced phosphorylation of IKKα/β, IκBα and p65 (Fig. S6b). The phosphorylation levels of JNK, ERK and p38 were elevated in LPS-treated BMDMs, and BBR significantly reversed MAPK activation (Fig. S6c).

SIRT3-silenced macrophages (SIRT3-KD) were generated to confirm the anti-inflammatory effects of BBR by activating SIRT3. The expression level of SIRT3 in knockdown cell line was 50% less than the cells expressing scrambled control shRNA (scrambled) (Fig. 6a). Compared to those of the scrambled control cells, the production of NO and the expression of iNOS (Fig. 6b, c) as well as the levels of IL-6, TNF-α and MCP-1 (Fig. 6d–f) were significantly induced by LPS stimulation in SIRT3-KD cells. As expected, the anti-inflammatory effects of BBR were partially abolished in LPS-challenged SIRT3-KD cells (Fig. 6b–f). The translocation of the NF-κB p65 subunit from the cytosol to the nucleus is involved in the regulation of inflammatory cytokines. The immunofluorescence images showed that BBR significantly suppressed p65 nuclear translocation in LPS-stimulated macrophages, and this effect was diminished by cotreatment with the SIRT3 inhibitor AGK7 (Fig. 6g). This effect was further confirmed by Western blot analysis (Fig. S7). These results demonstrate that BBR exerts anti-inflammatory effects at least partially by activating SIRT3 in macrophages.

BBR suppresses inflammatory responses by activating SIRT3 in adipocytes

To further characterize the role of SIRT3 in the BBR-mediated suppression of the inflammatory response in adipocytes, TNF-α-induced mature 3T3-L1 adipocytes were treated with BBR plus the SIRT3 inhibitor AGK7. As shown in Fig. 7a, the expression of iNOS and COX-2 was decreased, while SIRT3 expression was increased by BBR in TNF-α-induced adipocytes. Consistently, BBR dose-dependently reduced the acetylation levels in mitochondria from 3T3-L1 adipocytes (Fig. 7b), and this effect was blocked by cotreatment with cycloheximide (Fig. 7c). TNF-α induced NF-κB signalling activation in adipocytes, and BBR significantly suppressed the TNF-α-induced phosphorylation of IKKα/β, IκBα and p65 (Fig. 7d). Moreover, TNF-α also induced the phosphorylation of JNK, ERK and p38 in differentiated adipocytes, and BBR observably inhibited this activation (Fig. 7e). Notably, these effects of BBR were completely diminished in the presence of AGK7 (Fig. 7f–h). Thus, BBR suppresses TNF-α-mediated inflammation in differentiated adipocytes, at least partially by activating SIRT3.

DISCUSSION

During obesity, adipose tissue undergoes a variety of remodelling, resulting in unresolved chronic inflammation and fibrosis, which not only drives adipose tissue damage but also causes multiorgan dysfunction [27]. Pharmacological studies have shown that BBR alleviates differentiation, proliferation and adiposity by inhibiting galectin-3 expression in adipocytes [28], reduces lipid accumulation in adipocytes [29], enhances thermogenesis in white and brown adipose tissue [30], and alleviates adipose tissue fibrosis [31], largely by activating AMP-activated protein kinase (AMPK) signalling. In contrast, the beneficial effects of BBR on NAFLD are independent of AMPK [32]. A recent study indicated that BBR alleviates HFD-induced fatty acid β-oxidation inhibition via SIRT3-mediated LCAD (long-chain acyl-coenzyme A dehydrogenase) deacetylation [33]. Herein, we revealed that BBR alleviated inflammation and fibrosis in the adipose tissue of obese mice, to improve liver injury and insulin sensitivity.

ATMs play key roles in maintaining adipose tissue homeostasis and function in the healthy state by clearing cell debris and absorbing lipids from adipocytes, while under a positive energy state, long-term overactivation of ATMs results in chronic low-grade inflammation and a shift in the adipose immune landscape [6]. Pro-inflammatory cytokines are upregulated in WAT from genetically obese or diet induced obese mice prior to the development of IR [34]. BBR suppressed inflammatory cytokine and chemokine levels in the eWAT of HFD-fed mice, resulting in improvements in insulin sensitivity and systemic inflammation. M1/M2 macrophage polarization disorders are becoming the core mechanism of obesity pathogenesis and related comorbidities [35]. Selective ablation of M1 macrophages in obese mice decreases inflammatory markers and improves insulin sensitivity [36], while weight loss improves insulin sensitivity and induces the transient

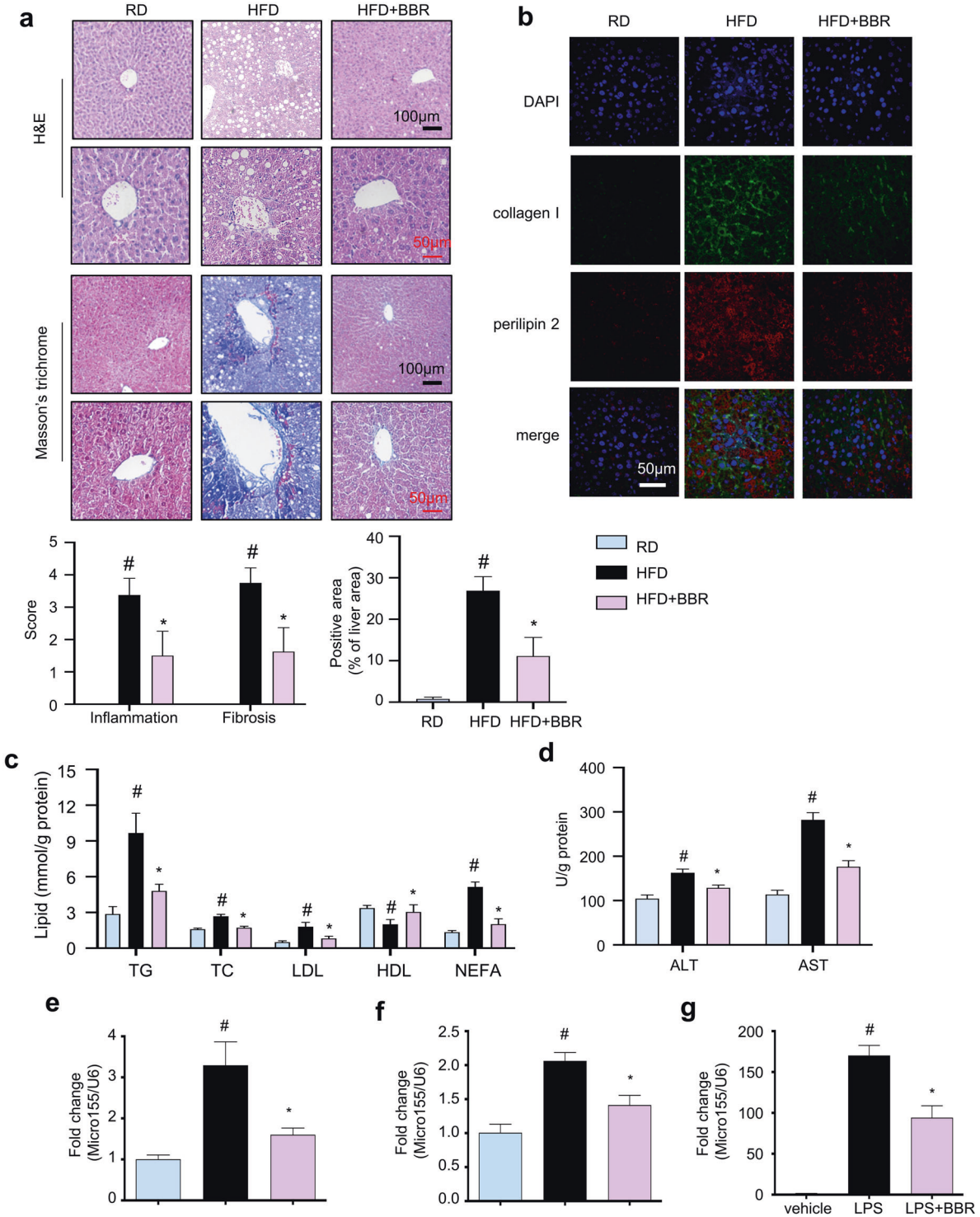

Fig. 4 BBR improves liver injury by suppressing the expression and secretion of *miR155-5p* in the ATMs of HFD-challenged mice. a H&E staining and Masson's trichrome staining of liver tissue sections (collagen: blue; nuclei: blue purple; cytoplasm: red). Scale bar (black) = 100 μm, scale bar (red) = 50 μm. Histopathological scores of portal inflammation and fibrosis in individual livers. 0 = no significant change, 1 = minimal, 2 = mild, 3 = moderate, and 4 = severe pathology. The proportion of positive-stained areas to total areas in Masson's trichrome-stained liver sections was estimated by ImageJ software. **b** Immunofluorescent staining of collagen I (green) and perilipin 2 (red) in liver tissue sections. Nuclei are stained with DAPI (blue). Scale bar (white) = 100 μm. **c** Lipids were extracted from the liver, and **d** the ALT and AST levels were measured. *miR-155-5p* levels in the serum (**e**) and eWAT (**f**) were measured and normalized to *U6* snRNA ($n = 8$). $^{\#}P < 0.05$ *vs*. HFD RD, $^{*}P < 0.05$ BBR *vs*. HFD. **g** The *miR-155-5p* levels were measured in LPS-challenged BMDMs ($n = 6$) and normalized to *U6* snRNA. The data represent the mean ± SD. $^{\#}P < 0.05$ LPS *vs*. vehicle, $^{*}P < 0.05$ BBR *vs*. LPS.

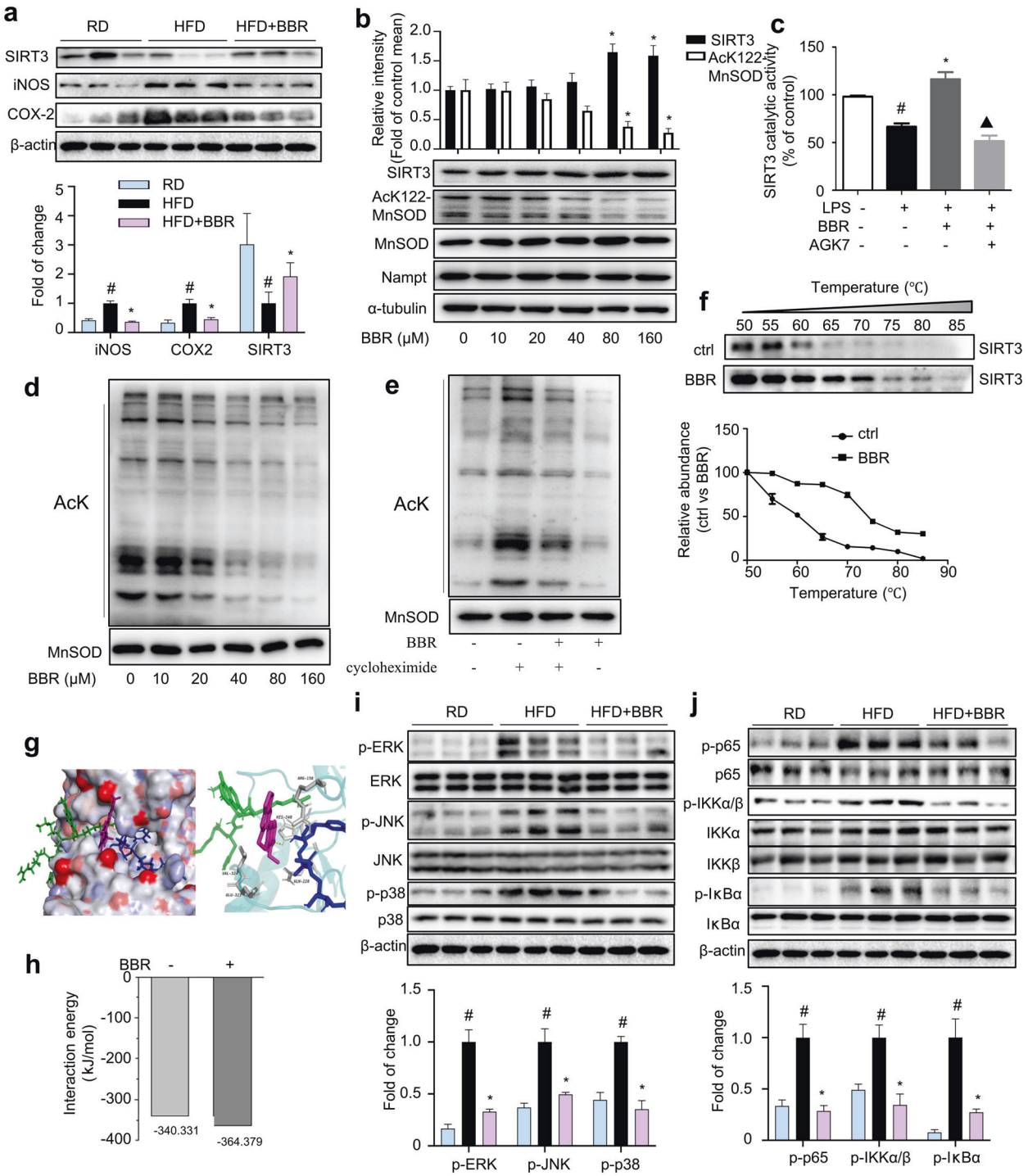

Fig. 5 BBR exacerbates SIRT3 activity and inhibits MAPK/NF-κB signalling in the eWAT of HFD-challenged mice. a The levels of iNOS, COX-2 and SIRT3 in eWAT were measured ($n = 8$). **b** Macrophages were treated with BBR (0–160 μM) for 24 h. SIRT3, AcK122 MnSOD, MnSOD and Nampt levels were measured ($n = 5$). $^{*}P < 0.05$ BBR *vs*. Control. **c** The effects of BBR on SIRT3 deacetylation activity were determined ($n = 6$). $^{\#}P < 0.05$ LPS *vs*. Control; $^{*}P < 0.05$ BBR *vs*. LPS; $^{\blacktriangle}P < 0.05$ AGK7 + BBR + LPS *vs*. BBR + LPS. **d** Mitochondrial lysates from macrophages treated with BBR were collected and evaluated for lysine acetylation using an anti-acetyl lysine antibody (AcK). MnSOD were used as a loading control. **e** Mitochondrial lysate from macrophages treated with cycloheximide (10 μM) for 1 h followed by treatment with BBR (80 μM) for an additional 2 h was analysed by Western blotting. **f** Cellular CETSA was performed on macrophages at different temperatures. The data were normalized to the mean value of the respective group at 50 °C ($n = 5$). **g** Predicted binding conformation of BBR to SIRT3 and interactions between BBR and SIRT3. **h** The calculated interaction energy between the substrate and protein in BBR-bound and BBR-free SIRT3. The expression levels of MAPKs (**i**) and NF-κB (**j**) were determined in eWAT ($n = 8$). The data represent the means ± SD. $^{\#}P < 0.05$ HFD *vs*. RD; $^{*}P < 0.05$ BBR *vs*. HFD.

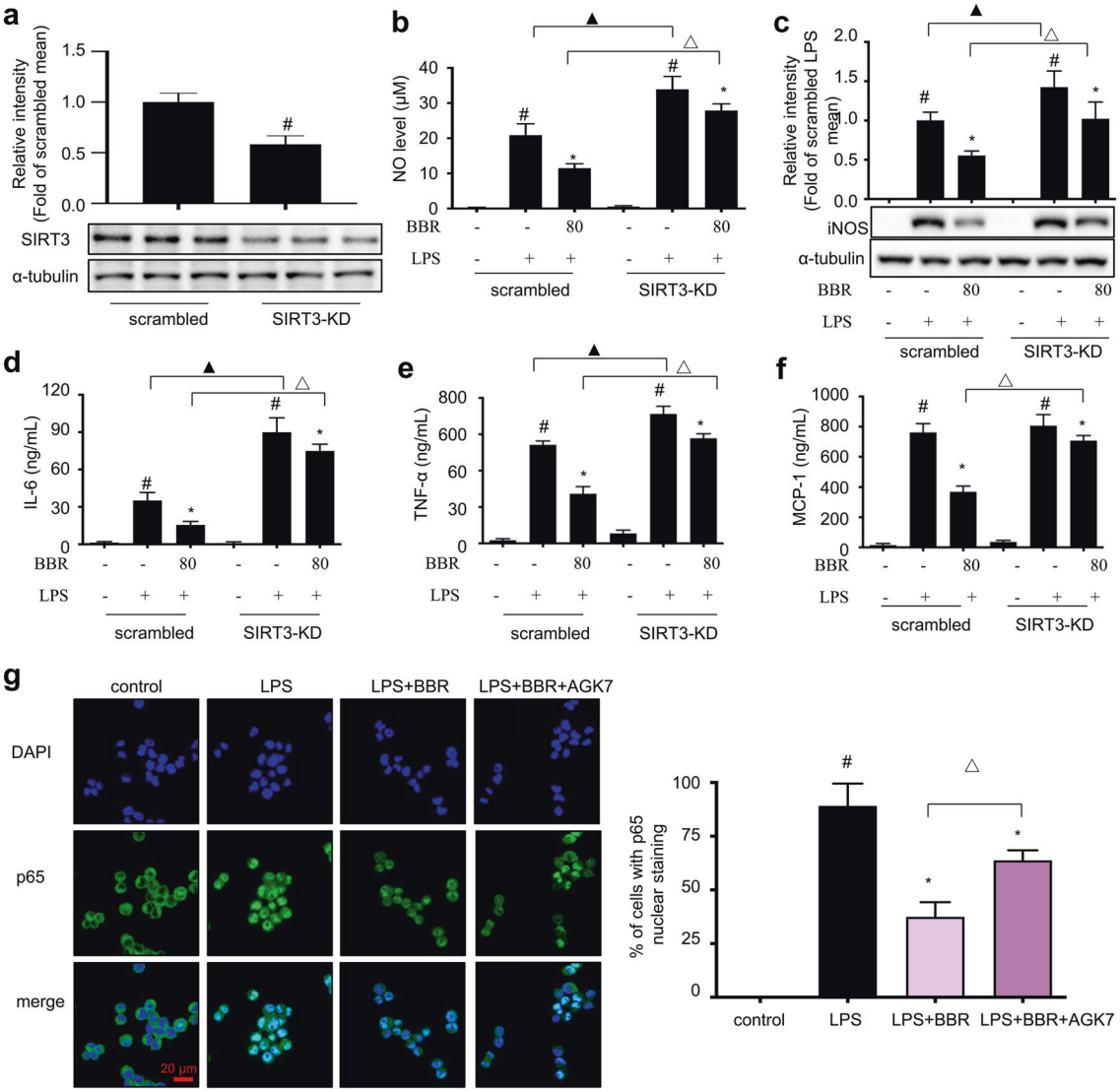

Fig. 6 SIRT3 knockdown reverses the anti-inflammatory effects of BBR on macrophages. a The expression level of SIRT3 was measured in SIRT3-KD macrophages and scrambled control cells. **b** NO production. **c** iNOS expression. The levels of IL-6 (**d**), TNF-α (**e**) and MCP-1 (**f**) were measured using ELISA kits. **g** Cells were pretreated with or without BBR and AGK7 and then exposed to LPS (1 μg/mL). The nuclear translocation of p65 was examined. Nuclei were stained with DAPI. Scale bar (white) = 20 μm. The data represent the means ± SD ($n = 6$). $^{\#}P < 0.05$ LPS *vs.* DMSO, $^{*}P < 0.05$ BBR *vs.* LPS, $^{\blacktriangle}P < 0.05$, SIRT3KD + LPS *vs.* scrambled + LPS, $^{\triangle}P < 0.05$ SIRT3KD + LPS + BBR *vs.* scrambled + LPS + BBR.

accumulation of M2 ATMs in mice [37]. BBR obviously promoted anti-inflammatory M2 macrophage polarization in both eWAT and IL-4-stimulated BMDMs. This evidence strongly suggests that BBR favours anti-inflammatory M2 macrophage polarization to alleviate HFD-induced adipose tissue inflammation.

In various pathological states, unresolved inflammation is often involved in altered tissue remodelling, and the persistence of inflammatory stress always progresses to fibrosis [9]. Fibrosis is characterized by the abnormal deposition of ECM components that result in severe organ dysfunction [38]. ECM components including collagens and fibronectin are needed for tissue mechanical development, while obesity-induced excessive production and abnormal deposition of ECM components gradually lead to destruction of the architecture of normal adipose tissue [8]. The loss of collagen genes in *ob/ob* mice leaves adipocyte expansion unimpeded and improves IR [39], while collagen expression in the adipose tissue of *db/db* mice is increased, which is further exacerbated by HFD feeding [40]. Consistent with these observations, the current study showed that collagen fibres formed bundles of various thicknesses, and thinner collagen fibrils appeared in the interstitial space of adipocytes, indicating pericellular fibrosis in the eWAT of HFD-induced obese mice. It is worth noting that there were thicker collagen fibres around hypertrophic adipocytes, which are located in the stromal space that is rich in macrophages, demonstrating that inflammation and fibrosis go hand-in-hand in the eWAT of obese mice. Interestingly, BBR reduced the levels of α-SMA and collagen I, thus ameliorating adipose tissue fibrosis. Furthermore, MMPs are a class of zinc-dependent proteases that are responsible for the degradation of collagen, and TIMPs are regulators of MMPs. Rigid fibrillar collagen networks are organized in the absence of MMP genes in adipose tissue, which affects the differentiation of adipocytes and the storage of lipids [41], and the deletion of TIMP genes results in obesity and IR in regular diet-fed mice and further exacerbates IR in HFD-fed mice [42]. BBR attenuated HFD-induced increases in MMP-9 and TIMP-1 in eWAT. These findings suggested that BBR could inhibit abnormal ECM synthesis and degradation in eWAT, which is beneficial for the healthy expansion of adipose tissue. Further research is needed to understand the mechanism by which BBR modulates ECM homeostasis.

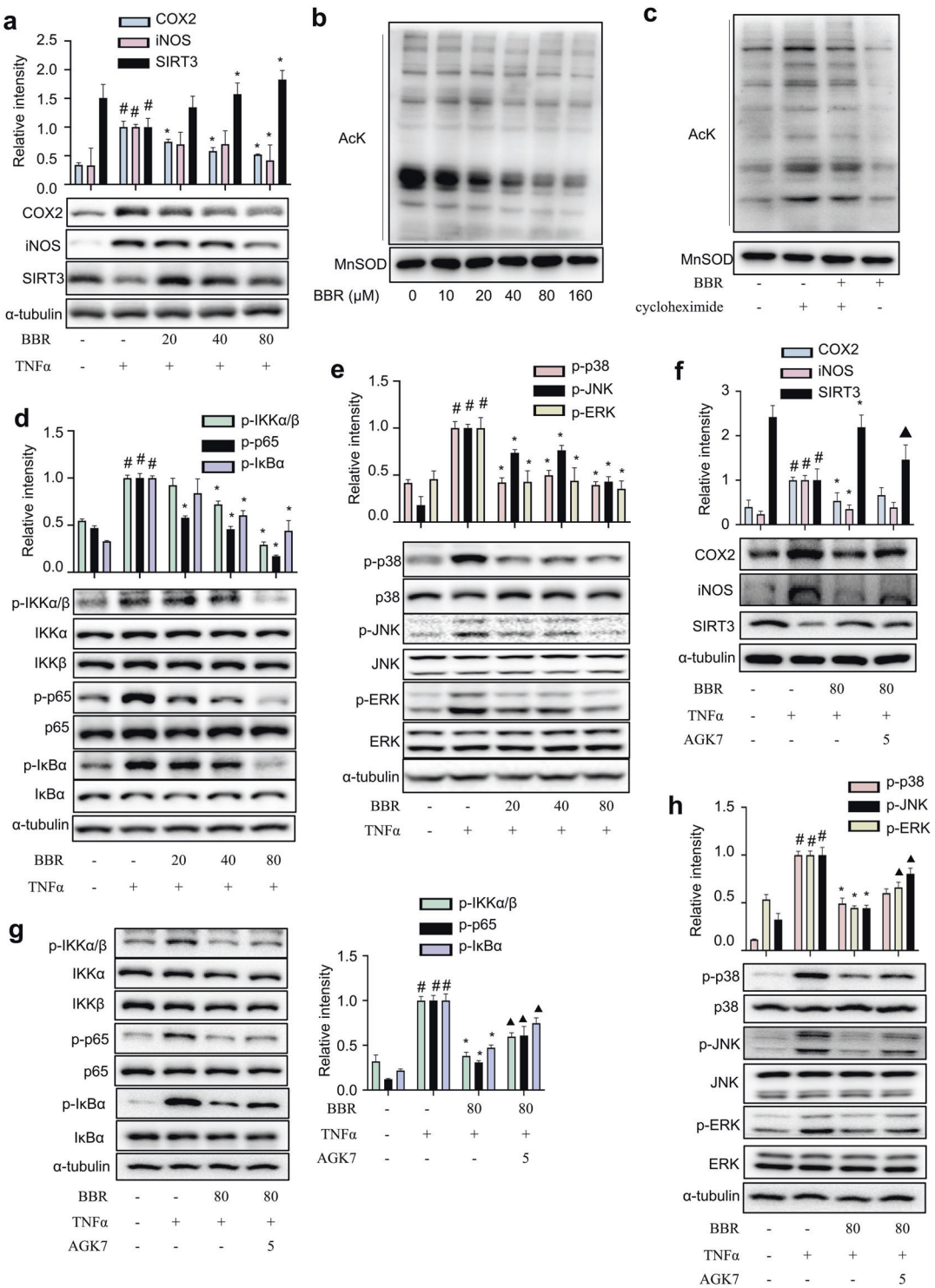

Fig. 7 SRIT3 suppression abrogates the anti-inflammatory effects of BBR on differentiated 3T3-L1 adipocytes. a Expression of iNOS, COX2, and SIRT3. **b** Mitochondrial lysates from differentiated adipocytes were treated with different doses of BBR and analysed for lysine acetylation using an anti-acetyl lysine antibody (AcK), and total MnSOD was used as a loading control. **c** Mitochondrial lysates from differentiated adipocytes treated with cycloheximide (10 μM) for 1 h followed by treatment with BBR (80 μM) for an additional 2 h were analysed by Western blotting. **d** Western blot analysis of NF-κB factors. α-Tubulin served as a loading control. **e** Western blot analysis of MAPKs factors. **f**–**h** The SIRT3 inhibitor AGK7 (5 μM) blocked the effects of BBR. The data represent the means ± SD ($n = 6$). $^{\#}P < 0.05$ TNF-α *vs*. DMSO, $^{*}P < 0.05$ BBR *vs*. TNF-α, $^{\blacktriangle}P < 0.05$ BBR + TNF-α + AGK7 *vs*. BBR + TNF-α.

Adipose tissue remodelling plays a critical role in the regulation of NAFLD and metabolic disorders in both animals and humans [43]. ATMs from patients with steatohepatitis secrete higher levels of cytokines and chemokines than ATMs from normal control subjects [44], indicating that omental inflammation leads to steatohepatitis by accelerating the production of inflammatory mediators in the portal system [45]. miRNAs are small noncoding RNA molecules that modulate mRNA expression and translational

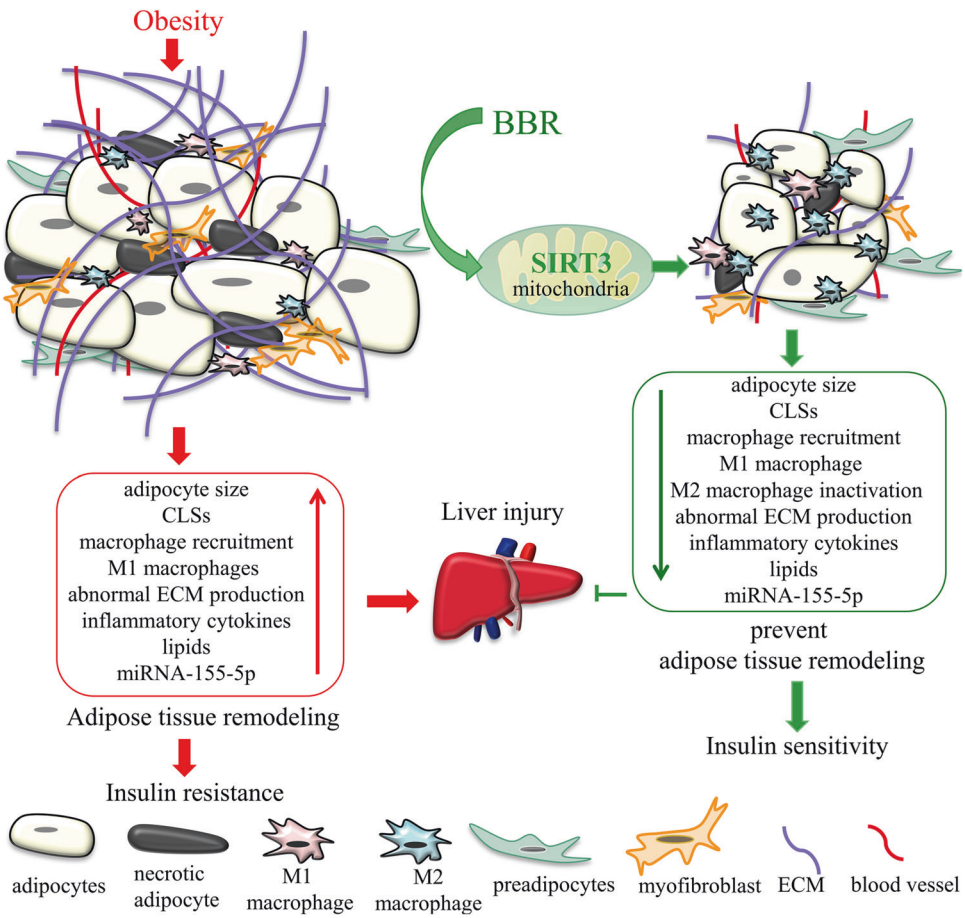

Fig. 8 The proposed mechanism of the beneficial effects of BBR on adipose tissue remodelling. Adipose tissue remodelling is characterized by pathologically uncontrolled adipocyte hypertrophy, excessive macrophage infiltration, abnormal ECM production and deposition, the secretion of inflammatory cytokines and miRNAs, liver injury and insulin resistance in the context of obesity. Therapeutically, BBR activates SIRT3 to suppress adipose tissue remodelling, which in turn alleviates liver injury, as well as systemic insulin resistance. The protective effect of BBR against liver injury might occur through the inhibition of *miRNA-155-5p* secretion by ATMs.

efficiency, and these factors could link adipose tissue inflammation, liver injury and IR during obesity [46]. Under obesity or HFD feeding, the miRNA expression profile of the whole body or local tissues is altered, and the target genes regulate insulin signalling pathways and glucose lipid metabolism, leading to the development of IR [47]. *miR-155* is a common target of multiple inflammatory mediators and is induced in macrophages under inflammatory conditions [23]. Selective knockout of *miR-155-5p* gene expression in macrophages ameliorates HFD-induced IR [46]. Additionally, serum/plasma miR-155 is dramatically elevated in the impaired liver [48], and silencing *miR-155* alleviates alcohol-induced steatohepatitis and fibrosis in the liver [24]. BBR inhibited the expression of *miR-155-5p* in ATMs from obese mice and LPS-stimulated BMDMs, which could protect against liver injury through the portal system. Further research is needed to understand the tissue-specific role of *miR-155-5p* in modulating adipose tissue homeostasis. The overexpression or knockdown of p65 in adipose tissue increases and decreases *miR-155* expression, respectively, suggesting that *miR-155* induction involves the NF-κB pathway [49]. These data strongly demonstrated that BBR could improve HFD-mediated liver injury at least partially by suppressing the secretion of *miR-155-5p* and pro-inflammatory cytokines by ATMs.

The deacetylase SIRT3 regulates mitochondrial biogenesis and function, and its expression level and activity are decreased in obesity [50]. Indeed, MitoTracker staining indicated that LPS and TNF-α significantly reduced mitochondrial levels compared with the controls, and BBR treatment markedly increased mitochondrial mass (Fig. S9a, b). JC-1 staining showed that the mitochondrial membrane potential in macrophages was interrupted by LPS, and BBR treatment significantly restored the mitochondrial membrane potential (Fig. S9c). Therefore, these results indicated that BBR enhances mitochondrial biogenesis and function in macrophages and adipocytes. Macrophages with SIRT3 silencing show elevated inflammation and M1 macrophage polarization [51]. SIRT3-deficient macrophages displayed impaired autophagy and accelerated NLRP3 inflammasome activation and endothelial dysfunction [52]. Dual deletion of SIRT2 and SIRT3 impacts the metabolism and inflammatory responses of macrophages and protects against endotoxemia [53]. To date, the role of SIRT3 in macrophages is not fully understood. SIRT3 depletion leads to adipocyte dysfunction and IR [54]. Herein, we found that the anti-inflammatory effect of BBR was abolished by SIRT3 inhibition or knockdown. Furthermore, SIRT3 knockout in HFD-fed mice results in accelerated obesity and metabolic syndrome [55], and the overexpression of SIRT3 in enterocytes of mice improves whole body glucose homeostasis and IR [56]. In our previous study, SIRT3 was downregulated in the eWAT of LPS-treated and ageing mice [12, 13]. As expected, BBR reversed the decline in SIRT3 expression in the eWAT of HFD-treated mice and exerted anti-inflammatory effects on LPS-stimulated macrophages and TNF-α-induced adipocytes by activating SIRT3.

AMPK mediates the protective effects of BBR against metabolic diseases. SIRT3 reduces lipid accumulation via AMPK activation in

human hepatic cells [57] and senses glucose levels [58]. SIRT3 deacetylates and activates liver kinase B1 (LKB1), which, in turn, stimulates AMPK activation [59]. Alternatively, SIRT3 promotes increases in cytosolic calcium levels, which activates calcium/calmodulin-dependent kinase II (CaMKII) to phosphorylate AMPK [60]. As expected, the phosphorylation levels of AMPK were reduced in LPS-induced macrophages and TNF-α-stimulated adipocytes; BBR activated AMPK in both cell models, and this effect was partially blocked by cotreatment with Compound C, an AMPK inhibitor (Fig. S10). These results reveal that BBR activates the SIRT3-AMPK pathway.

The MAPK and NF-κB signalling pathways are negative feedback controlled by SIRT3 [26, 61] and are positively correlated with the level of miRNA-155 [62]. In our study, *miRNA-155-5p* was increased in the serum and eWAT of obese mice and LPS-induced macrophages, suggesting that the relationship between SIRT3 and *miRNA-155-5p* might be negative in the context of inflammation and obesity. Further studies are needed to confirm this relationship. These data demonstrate that BBR improves adipose tissue remodelling by activating SIRT3 expression, which is an important negative regulator of M1 macrophage polarization and *miRNA-155-5p* secretion and contributes to prevent obesity related metabolic disorders.

Our study reveals that pharmacological activation of SIRT3 by BBR effectively ameliorates adipose tissue remodelling in HFD-induced obese mice and subsequently inhibits *miR-155-5p* secretion from macrophages, which in turn protects mice against liver injury and systemic IR (Fig. 8). These findings further verified that BBR could be a promising candidate to treat obesity-related metabolic disorders.

ACKNOWLEDGEMENTS

Financial support was provided by the National Natural Science Foundation of China (81872754, 81630101 and 81891012), the Science and Technology Development Fund, Macao SAR (File no. FDCT 0031/2019/A1), the Research Fund of University of Macau (MYRG2018-00037-ICMS and MYRG2020-00091-ICMS), the Genetics Innovation Platform of Southwestern Chinese Medicine Resources (2020ZYD058), the Open Research Fund of Chengdu University of Traditional Chinese Medicine Key Laboratory of Systematic Research of Distinctive Chinese Medicine Resources in Southwest China (2020GZ2011011 and 2020BSH004), special support from the China Postdoctoral Science Foundation (2019M663456 and 2019TQ0044), the Xinglin Scholar Research Promotion Project of Chengdu University of TCM (BSH2019008), and the Sichuan Province Science and Technology Innovation Seedling Project (2020091).

AUTHOR CONTRIBUTIONS

DL, CY, JZZ, EL, and TZ conducted the experiments; DL, QT, CP and LGL designed the experiments and wrote the paper; and LGL conceived the study.

ADDITIONAL INFORMATION

Supplementary information The online version contains supplementary material available at https://doi.org/10.1038/s41401-021-00736-y.

Competing interests: The authors declare no conflicts of interests.

REFERENCES

1. Stefan N. Causes, consequences, and treatment of metabolically unhealthy fat distribution. Lancet Diabetes Endocrinol. 2020;8:616–27.
2. Sun K, Kusminski CM, Scherer PE. Adipose tissue remodeling and obesity. J Clin Invest. 2011;121:2094–101.
3. Lee MJ, Wu Y, Fried SK. Adipose tissue remodeling in pathophysiology of obesity. Curr Opin Clin Nutr Metab Care. 2010;13:371–6.
4. Maury E, Noel L, Detry R, Brichard SM. In vitro hyperresponsiveness to tumor necrosis factor-alpha contributes to adipokine dysregulation in omental adipocytes of obese subjects. J Clin Endocrinol Metab. 2009;94:1393–400.
5. Weisberg SP, McCann D, Desai M, Rosenbaum M, Leibel RL, Ferrante AW. Obesity is associated with macrophage accumulation in adipose tissue. J Clin Invest. 2003;112:1796–808.
6. Catrysse L, van Loo G. Adipose tissue macrophages and their polarization in health and obesity. Cell Immunol. 2018;330:114–9.
7. Russo L, Lumeng CN. Properties and functions of adipose tissue macrophages in obesity. Immunology. 2018;155:407–17.
8. Luo T, Nocon A, Fry J, Sherban A, Rui X, Jiang B, et al. AMPK activation by metformin suppresses abnormal extracellular matrix remodeling in adipose tissue and ameliorates insulin resistance in obesity. Diabetes. 2016;65:2295–310.
9. Marcelin G, Silveira ALM, Martins LB, Ferreira AV, Clement K. Deciphering the cellular interplays underlying obesity-induced adipose tissue fibrosis. J Clin Invest. 2019;129:4032–40.
10. Cicero AF, Baggioni A. Berberine and its role in chronic disease. Adv Exp Med Biol. 2016;928:27–45.
11. Kong WJ, Vernieri C, Foiani M, Jiang JD. Berberine in the treatment of metabolism-related chronic diseases: A drug cloud (dCloud) effect to target multifactorial disorders. Pharmacol Ther. 2020;209:107496.
12. Li D, Liu Q, Sun W, Chen X, Wang Y, Sun Y, et al. 1,3,6,7-Tetrahydroxy-8-prenylxanthone ameliorates inflammatory responses resulting from the paracrine interaction of adipocytes and macrophages. Br J Pharmacol. 2018;175:1590–606.
13. Li D, Liu Q, Lu X, Li Z, Wang C, Leung CH, et al. alpha-Mangostin remodels visceral adipose tissue inflammation to ameliorate age-related metabolic disorders in mice. Aging. 2019;11:11084–110.
14. Shen S, Liao Q, Zhang T, Pan R, Lin L. Myricanol modulates skeletal muscle-adipose tissue crosstalk to alleviate high-fat diet-induced obesity and insulin resistance. Br J Pharmacol. 2019;176:3983–4001.
15. Zhang T, Fang Z, Linghu K, Liu J, Gan L, Lin L. Small molecule-driven SIRT3-autophagy-mediated NLRP3 inflammasome inhibition ameliorates inflammatory crosstalk between macrophages and adipocytes. Br J Pharmacol. 2020;177:4645–65.
16. Zhang L, Guo J, Jiang X, Chen X, Wang Y, Li A, et al. Identification of nagilactone E as a protein synthesis inhibitor with anticancer activity. Acta Pharmacol Sin. 2020;41:698–705.
17. Jafari R, Almqvist H, Axelsson H, Ignatushchenko M, Lundback T, Nordlund P, et al. The cellular thermal shift assay for evaluating drug target interactions in cells. Nat Protoc. 2014;9:2100–22.
18. Martinez Molina D, Jafari R, Ignatushchenko M, Seki T, Larsson EA, Dan C, et al. Monitoring drug target engagement in cells and tissues using the cellular thermal shift assay. Science. 2013;341:84–7.
19. Maier JA, Martinez C, Kasavajhala K, Wickstrom L, Hauser KE, Simmerling C. ff14SB: Improving the accuracy of protein side chain and backbone parameters from ff99SB. J Chem Theory Comput. 2015;11:3696–713.
20. Jakalian A, Jack DB, Bayly CI. Fast, efficient generation of high-quality atomic charges. AM1-BCC model: II. Parameterization and validation. J Comput Chem. 2002;23:1623–41.
21. Wang J, Wolf RM, Caldwell JW, Kollman PA, Case DA. Development and testing of a general amber force field. J Comput Chem. 2004;25:1157–74.
22. Madura JorgensenC, Impey & Klein. Comparison of simple potential functions for simulating liquid water. J Chem Phys. 1983;78:926–35.
23. O'connell RM, Taganov KD, Boldin MP, Cheng GH, Baltimore D. MicroRNA-155 is induced during the macrophage inflammatory response. Proc Natl Acad Sci USA. 2007;104:1604–9.
24. Bala S, Csak T, Saha B, Zatsiorsky J, Kodys K, Catalano D, et al. The pro-inflammatory effects of miR-155 promote liver fibrosis and alcohol-induced steatohepatitis. J Hepatol. 2016;64:1378–87.
25. Quan Y, Park W, Jin J, Kim W, Park SK, Kang KP. Sirtuin 3 activation by honokiol decreases unilateral ureteral obstruction-induced renal inflammation and fibrosis via regulation of mitochondrial dynamics and the renal NF-κB/TGF-β1/Smad signaling pathway. Int J Mol Sci. 2020;21:402.
26. Sundaresan NR, Gupta M, Kim G, Rajamohan SB, Isbatan A, Gupta MP. Sirt3 blocks the cardiac hypertrophic response by augmenting Foxo3a-dependent antioxidant defense mechanisms in mice. J Clin Invest. 2009;119:2758–71.
27. Li D, Zhang T, Lu J, Peng C, Lin L. Natural constituents from food sources as therapeutic agents for obesity and metabolic diseases targeting adipose tissue inflammation. Crit Rev Food Sci Nutr. 2021;61:1947–65.
28. Wang C, Wang Y, Ma SR, Zuo ZY, Wu YB, Kong WJ, et al. Berberine inhibits adipocyte differentiation, proliferation and adiposity through down-regulating galectin-3. Sci Rep. 2019;9:13415.
29. Lee YS, Kim WS, Kim KH, Yoon MJ, Cho HJ, Shen Y, et al. Berberine, a natural plant product, activates AMP-activated protein kinase with beneficial metabolic effects in diabetic and insulin-resistant states. Diabetes. 2006;55:2256–64.
30. Zhang Z, Zhang H, Li B, Meng X, Wang J, Zhang Y, et al. Berberine activates thermogenesis in white and brown adipose tissue. Nat Commun. 2014;5:5493.
31. Wang L, Ye X, Hua Y, Song Y. Berberine alleviates adipose tissue fibrosis by inducing AMP-activated kinase signaling in high-fat diet-induced obese mice. Biomed Pharmacother. 2018;105:121–9.

32. Guo T, Woo SL, Guo X, Li H, Zheng J, Botchlett R, et al. Berberine ameliorates hepatic steatosis and suppresses liver and adipose tissue inflammation in mice with diet-induced obesity. Sci Rep. 2016;6:22612.
33. Xu X, Zhu XP, Bai JY, Xia P, Li Y, Lu Y, et al. Berberine alleviates nonalcoholic fatty liver induced by a high-fat diet in mice by activating SIRT3. FASEB J. 2019;33:7289–300.
34. Xu H, Barnes GT, Yang Q, Tan G, Yang D, Chou CJ, et al. Chronic inflammation in fat plays a crucial role in the development of obesity-related insulin resistance. J Clin Invest. 2003;112:1821–30.
35. Thomas D, Apovian C. Macrophage functions in lean and obese adipose tissue. Metabolism. 2017;72:120–43.
36. Patsouris D, Li PP, Thapar D, Chapman J, Olefsky JM, Neels JG. Ablation of CD11c-positive cells normalizes insulin sensitivity in obese insulin resistant animals. Cell Metab. 2008;8:301–9.
37. Kosteli A, Sugaru E, Haemmerle G, Martin JF, Lei J, Zechner R, et al. Weight loss and lipolysis promote a dynamic immune response in murine adipose tissue. J Clin Invest. 2010;120:3466–79.
38. Wynn TA, Ramalingam TR. Mechanisms of fibrosis: therapeutic translation for fibrotic disease. Nat Med. 2012;18:1028–40.
39. Shen M, Kumar SP, Shi H. Estradiol regulates insulin signaling and inflammation in adipose tissue. Horm Mol Biol Clin Investig. 2014;17:99–107.
40. Huber J, Loffler M, Bilban M, Reimers M, Kadl A, Todoric J, et al. Prevention of high-fat diet-induced adipose tissue remodeling in obese diabetic mice by n-3 polyunsaturated fatty acids. Int J Obes. 2007;31:1004–13.
41. Chun TH, Hotary KB, Sabeh F, Saltiel AR, Allen ED, Weiss SJ. A pericellular collagenase directs the 3-dimensional development of white adipose tissue. Cell. 2006;125:577–91.
42. Jaworski DM, Sideleva O, Stradecki HM, Langlois GD, Habibovic A, Satish B, et al. Sexually dimorphic diet-induced insulin resistance in obese tissue inhibitor of metalloproteinase-2 (TIMP-2)-deficient mice. Endocrinology. 2011;152:1300–13.
43. Azzu V, Vacca M, Virtue S, Allison M, Vidal-Puig A. Adipose tissue-liver cross talk in the control of whole-body metabolism: Implications in nonalcoholic fatty liver disease. Gastroenterology. 2020;158:1899–912.
44. du Plessis J, van Pelt J, Korf H, Mathieu C, van der Schueren B, Lannoo M, et al. Association of adipose tissue inflammation with histologic severity of nonalcoholic fatty liver disease. Gastroenterology. 2015;149:635–48.
45. Petta S, Amato MC, Di Marco V, Camma C, Pizzolanti G, Barcellona MR, et al. Visceral adiposity index is associated with significant fibrosis in patients with non-alcoholic fatty liver disease. Aliment Pharmacol Ther. 2012;35:238–47.
46. Ying W, Riopel M, Bandyopadhyay G, Dong Y, Birmingham A, Seo JB, et al. Adipose tissue macrophage-derived exosomal miRNAs can modulate in vivo and in vitro insulin sensitivity. Cell. 2017;171:372–84.
47. Pan Y, Hui X, Hoo RLC, Ye D, Chan CYC, Feng T, et al. Adipocyte-secreted exosomal microRNA-34a inhibits M2 macrophage polarization to promote obesity-induced adipose inflammation. J Clin Invest. 2019;129:834–49.
48. Bala S, Petrasek J, Mundkur S, Catalano D, Levin I, Ward J, et al. Circulating microRNAs in exosomes indicate hepatocyte injury and inflammation in alcoholic, drug-induced, and inflammatory liver diseases. Hepatology. 2012;56:1946–57.
49. Karkeni E, Astier J, Tourniaire F, El Abed M, Romier B, Gouranton E, et al. Obesity-associated inflammation induces microRNA-155 expression in adipocytes and adipose tissue: outcome on adipocyte function. J Clin Endocrinol Metab. 2016;101:1615–26.
50. Kwon S, Seok S, Yau P, Li X, Kemper B, Kemper JK. Obesity and aging diminish sirtuin 1 (SIRT1)-mediated deacetylation of SIRT3, leading to hyperacetylation and decreased activity and stability of SIRT3. J Biol Chem. 2017;292:17312–23.
51. Xu H, Hertzel AV, Steen KA, Bernlohr DA. Loss of fatty acid binding protein 4/aP2 reduces macrophage inflammation through activation of SIRT3. Mol Endocrinol. 2016;30:325–34.
52. Liu P, Huang G, Wei T, Gao J, Huang C, Sun M, et al. Sirtuin 3-induced macrophage autophagy in regulating NLRP3 inflammasome activation. Biochim Biophys Acta Mol Basis Dis. 2018;1864:764–77.
53. Heinonen T, Ciarlo E, Rigoni E, Regina J, Le Roy D, Roger T. Dual Deletion of the Sirtuins SIRT2 and SIRT3 impacts on metabolism and inflammatory responses of macrophages and protects from endotoxemia. Front Immunol. 2019;10:2713.
54. Wu YT, Chi KT, Lan YW, Chan JC, Ma YS, Wei YH. Depletion of Sirt3 leads to the impairment of adipogenic differentiation and insulin resistance via interfering mitochondrial function of adipose-derived human mesenchymal stem cells. Free Radic Res. 2018;52:1398–415.
55. Hirschey MD, Shimazu T, Jing E, Grueter CA, Collins AM, Aouizerat B, et al. SIRT3 deficiency and mitochondrial protein hyperacetylation accelerate the development of the metabolic syndrome. Mol Cell. 2011;44:177–90.
56. Ramachandran D, Clara R, Fedele S, Hu J, Lackzo E, Huang JY, et al. Intestinal SIRT3 overexpression in mice improves whole body glucose homeostasis independent of body weight. Mol Metab. 2017;6:1264–73.
57. Shi T, Fan GQ, Xiao SD. SIRT3 reduces lipid accumulation via AMPK activation in human hepatic cells. J Dig Dis. 2010;11:55–62.
58. Palacios OM, Carmona JJ, Michan S, Chen KY, Manabe Y, Ward JL 3rd, et al. Diet and exercise signals regulate SIRT3 and activate AMPK and PGC-1alpha in skeletal muscle. Aging. 2009;1:771–83.
59. Pillai VB, Sundaresan NR, Kim G, Gupta M, Rajamohan SB, Pillai JB, et al. Exogenous NAD blocks cardiac hypertrophic response via activation of the SIRT3-LKB1-AMP-activated kinase pathway. J Biol Chem. 2010;285:3133–44.
60. Woods A, Dickerson K, Heath R, Hong SP, Momcilovic M, Johnstone SR, et al. Ca^{2+}/calmodulin-dependent protein kinase kinase-beta acts upstream of AMP-activated protein kinase in mammalian cells. Cell Metab. 2005;2:21–33.
61. Gao J, Chen N, Li N, Xu F, Wang W, Lei Y, et al. Neuroprotective effects of trilobatin, a novel naturally occurring Sirt3 agonist from *Lithocarpus polystachyus* Rehd., mitigate cerebral ischemia/reperfusion injury: involvement of TLR4/NF-kappaB and Nrf2/Keap-1 signaling. Antioxid Redox Signal. 2020;33:117–43.
62. Duan Z, Zhang J, Li J, Pang X, Wang H. Inhibition of microRNA-155 reduces neuropathic pain during chemotherapeutic bortezomib via engagement of neuroinflammation. Front Oncol. 2020;10:416.